Investigating Dual Electrospinning as a Means of Enhancing Passive Thermal Control Coatings for Cryogenic Propellant Storage in Extraterrestrial Environments

Chieloka Ibekwe[1], Adrien Neveu[1], Nan An[1], Xuanjie Wang[1], Jason Hartwig[2], Adam Swanger[3] and Shankar Narayan[1*]

[1] Department of Mechanical, Aerospace and Nuclear Engineering, Rensselaer Polytechnic Institute, Troy, NY 12180, USA
[2] NASA Glenn Research Center, Cleveland, OH 44135, USA
[3] NASA Kennedy Space Center, Cryogenics Test Laboratory, FL 32899, USA

[*]E-mail: narays5@rpi.edu

Abstract. Passive thermal control is necessary as space exploration becomes increasingly widespread. Materials with superior optical properties (high solar reflectance and infrared emittance) are critical for passive thermal control because they can reject most of the incident solar radiation and promote thermal emission from cryogenic propellant storage tanks, enabling the extraterrestrial storage of cryogens. We have demonstrated in previous studies that electrospun nanofibers exhibit exceptional optical properties, offering significant benefits for passive radiative cooling in space. Particularly, electrospun polyvinylidene fluoride-co-hexafluoropropylene PVDF-HFP nanofibers demonstrate exceptionally high solar reflectance (>99%) and strong thermal emittance (measured at ~300 K). However, they exhibit nanostructural changes in the presence of atomic oxygen, which is prevalent in Low Earth Orbit. This study focuses on creating a unique blend of polymeric (PVDF-HFP) and ceramic-based (silica) nanofibers by leveraging the chemical stability and atomic oxygen resistance of silica, using the dual electrospinning manufacturing method. This approach aims to preserve the structural properties of the polymeric counterpart without compromising its optical performance, thereby providing an innovative method for manufacturing environmentally resilient passive thermal control nanofibers with desirable optical and thermal control functionalities for extraterrestrial storage of cryogenic propellants.

1. Introduction

As space exploration becomes more prevalent, passive thermal control becomes increasingly necessary. Storage of cryogenic compressed fuels in space must be exposed to as little thermal energy as possible, and the primary method of accomplishing this task is through the reflection of incident sunlight. Current passive reflective thermal control materials are typically metallic, with relatively high reflectivity; however, their absorptive properties result in high surface coating temperatures after prolonged exposure to sunlight. This shortcoming necessitates the use of active cooling techniques, which are non-ideal for payload efficiency. In this regard, next-generation thermal coatings can have a significant role. Previous studies [1–3] have demonstrated that electrospun nanofibers with high solar reflectance and infrared emittance exhibit a passive cooling phenomenon even when exposed to direct solar radiation.

This study aims to create hybrid electrospun materials through dual spinning, leveraging the desirable traits of two different electrospun materials while minimizing their undesirable traits.

Individually, different materials show promise as reflective insulators, but with distinct drawbacks. The polymer-based nanofibrous thermal control material made from polyvinylidene fluoride-co-hexafluoropropylene (PVDF-HFP) co-polymer is a highly effective radiative thermal insulator with very high reflectivity (average solar reflectance greater than 99%). However, this material experiences structural degradation by coalescing into microfibers in the presence of atomic oxygen, which could adversely affect its optical properties. Conversely, silica-based nanofibers [2], with average solar reflectance averaging ~97%, are highly resistant to atomic oxygen. Atomic oxygen (AO) is prevalent in Low Earth orbit (LEO) due to the photodissociation of molecular oxygen in the Earth's upper atmosphere by highly energetic ultraviolet radiation [4–8]. Its high reactivity makes it a significant contributor to the degradation of spacecraft materials, hence the need to design and manufacture AO-resistant materials with desirable thermal control functionalities.

This research aims to interweave highly reflective PVDF-HFP nanofibers with AO-resistant silica nanofibers through dual electrospinning, to maintain the reflective performance of the polymeric constituent while incorporating the atomic oxygen resistance of silica. The goals for the resultant composite dual electrospun material are to achieve a reflectivity comparable to that of the PVDF-HFP electrospun fibers, while also being more resilient to atomic oxygen than the polymeric precursor material.

2. Methodology

2.1 Materials and Preparation of Precursor Solutions

Polyvinylidene fluoride-co-hexafluoropropylene and tetraethyl orthosilicate were obtained from Sigma-Aldrich. N,N-Dimethylformamide (DMF) solvent was purchased from Spectrum Chemical, and acetone was obtained from VWR Chemicals BDH. Ethanol was obtained from Decon Labs, and hydrochloric acid from Fisher Scientific.

PVDF-HFP solution was prepared by dissolving the PVDF-HFP pellets in a solution of dimethyl formamide (DMF) and acetone (70/30 w/w) to form an 18% wt. solution. The solution was stirred at 40 ℃ and 400 rpm for 5 hours to form a viscous PVDF-HFP solution for electrospinning. A silica solution was prepared by mixing tetraethyl orthosilicate, ethanol, deionized water, and a 37% aqueous solution of hydrochloric acid. This mixture was stirred at 40 ℃ and 200 rpm for six hours to ensure thorough mixing. After preparation, both solutions were transferred into separate syringes for the dual electrospinning process.

2.2 Manufacturing and Characterization of Dual-electrospun Nanofibers

The dual electrospinning process for creating interwoven nanofibers requires the setup shown in Figure 1(a). Two high-voltage power supplies (set to 20 kV), two syringe pumps (set to 1 ml/hr), syringes, needles, and an electrically grounded rotating collector overlayed with aluminum foil were used in this process. The spinnerets were positioned on opposite sides of the collector to deposit their constituent nanofibers simultaneously onto the collector. Similar flow rates were used to produce a material with a uniform ratio of PVDF-HFP and silica nanofibers. Although initial studies did not systematically tune the ratios of the constituent polymers, subsequent studies would involve a detailed analysis of the effects of the ratios of both materials on the properties of the composite.

The production of nanofibers from each spinneret follows the same process as a single electrospinning process [9–11]; slight modifications, however, exist. Positive biases applied to the opposite-facing needles, intercepted by a grounded collector that was equally distant from both needles, resulted in very high potential differences between each needle and the collector. This led to the

formation of Taylor cones at the tips of the needles, ejecting liquid jets which formed solid nanofibers as they dried out while traveling towards the collector. These nanofibers were deposited on the aluminum foil substrate, forming a thick, white coating of dual-spun PVDF-HFP-silica nanofibers, as seen in Figure 1(b). At the end of the deposition process, having allowed sufficient time for drying, their properties were characterized.

The morphology of the dual-spun nanofibrous material was characterized using a Carl Zeiss Supra 55 Field Emission Scanning Electron Microscope (FESEM), and the micrographs were analyzed using Image J software to obtain the nanofiber distribution. Spectral hemispherical reflectance measurements were taken in the 300-2500 nm solar wavelength range using a Perkin-Elmer Lambda 950 UV-Visible-NIR spectrophotometer interfaced with a 6-inch thick Spectralon® integrating sphere accessory. The average solar reflectance (ρ_s) of the material was calculated using Equation 1 below:

$$\rho_S = \frac{\int_{\lambda_1=300\ nm}^{\lambda_2=2500\ nm} \rho_s(\lambda)\, I_s(\lambda) d\lambda}{\int_{\lambda_1=300\ nm}^{\lambda_2=2500\ nm} I_s(\lambda) d\lambda} \quad (1)$$

Here, $I_s(\lambda)$ represents the extraterrestrial solar spectral intensity (Air Mass 0 or AM 0) and $\rho_s(\lambda)$ represents the spectral hemispherical reflectance obtained from the spectrophotometer, relative to Spectralon's® reflectance. The mid infrared (2.5-15 μm) spectral reflectance and transmittance were characterized using a Fourier-Transform Infrared spectrometer (ThermoFisher Scientific Nicolet™ iS20) equipped with a 3-inch gold-coated integrating sphere (Pike Technologies Mid-IR IntegratIR™) and a mercury cadmium telluride (MCT) detector. The measured reflectance $\rho_s(\lambda)$ and transmittance ($\tau_s(\lambda)$) was used to obtain the emittance as $\varepsilon_{IR,\lambda} = 1 - \rho_s(\lambda) - \tau_s(\lambda)$. The average emittance (ε_{IR}) of the material was calculated using:

$$\varepsilon_{IR} = \frac{\int_{\lambda_1=2.5\ \mu m}^{\lambda_2=15\ \mu m} (\varepsilon_{IR,\lambda})\, E_{b\lambda}(\lambda,T) d\lambda}{\int_{\lambda_1=2.5\ \mu m}^{\lambda_2=15\ \mu m} E_{b\lambda}(\lambda,T) d\lambda} \quad (2)$$

$$E_{b\lambda}(\lambda,T) = \frac{2hc^2}{\lambda^5 (e^{\frac{hc}{\lambda K_B T}} - 1)} \quad (3)$$

where $\varepsilon_{IR,\lambda}$ describes the spectral hemispherical emittance and $E_{b\lambda}(\lambda,T)$ is the Planck's spectral blackbody emissive radiance. h, c, λ, K_B, T represent Planck's constant, speed of light in vacuum, wavelength, Boltzmann's constant, and absolute temperature of the blackbody, respectively.

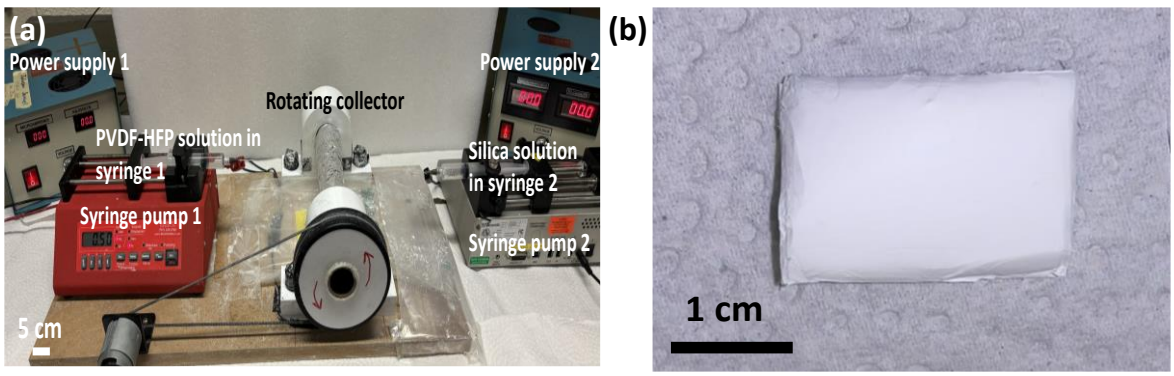

Figure 1. (a) Dual electrospinning setup to produce the PVDF-HFP – silica nanofibrous composite. (b) An image of the dual-spun material cut from a larger piece.

2.3 Extraterrestrial Environment Durability – Atomic Oxygen and Thermal Cycling

The extreme conditions in space can degrade space-exposed materials, which necessitate numerous testing and validation procedures to qualify materials for space use. Ground-based experiments are

important because they provide engineers and scientists with valuable data to guide the material development process before launching these materials into space for long-duration exposure experiments. Accordingly, we performed atomic oxygen and thermal cycling experiments on the dual-spun materials to characterize their resilience.

To test the AO-resistance of the material, we re-purposed a radio frequency (RF 13.56 MHz) plasma device (Harrick Plasma, PDC-32G) interfaced with oxygen process gas. The oxygen plasma produced during operation consists of different charged and neutral species (including ions, radicals, and neutral atomic oxygen). We used a Faraday box [12–14] to shield the dual-spun sample from the charged species in the plasma, permitting only AO to interact with the material. Kapton, whose erosion rate in Low Earth Orbit has been extensively characterized, was used as a witness sample for comparison. A chamber pressure of 0.9 Torr was maintained in the plasma chamber during the test, and the samples were exposed for 24 hours.

Materials can experience extreme thermal cycling (between cryogenic and high temperatures) when they move from facing the cosmic dark background to direct solar exposure. These lead to thermally induced stresses, which could impair the material properties. Therefore, we conducted thermal cycling on the dual-spun material by inserting it in a bath of liquid nitrogen (-196 ^{o}C) and allowing the material to cool rapidly and attain cryogenic temperatures. After ~5 minutes, the material was transferred to a convection furnace set to 100 ^{o}C, resulting in a rapid temperature rise. These rapid cycles simulate the extraterrestrial environment where materials may not have sufficient time to dissipate thermally induced stresses as they transition from one thermal environment to another. Following these tests, we characterize the material's properties and discuss the results in the subsequent sections.

3. Results and Discussion

3.1 Morphology, Structure and Optical Properties

Figure 2 shows the morphology and structure of the three electrospun materials. Figure 2(a) shows PVDF-HFP nanofibers, Figure 2(b) shows silica nanofibers, and Figure 2(c) shows the dual-spun PVDF-HFP-silica composite nanofibers. All three materials have porous structures with randomly oriented nanoscale fibers. Particularly, Figure 2(d) illustrates the range of distribution of fiber diameters for the dual-spun composite material. We observe that most of the fiber sizes fall within the wavelengths of the solar spectrum, and the interaction of light propagating through the material would be governed by Mie scattering [15]. This wavelength-dependent scattering of light in all directions would impart strong diffusely reflective characteristics to the material. Additionally, contrasting refractive indices, which exist between the nanofibers and air-filled pores across the thickness of the fibrous network, enhance light scattering. This is another significant contributor to the markedly high solar reflectance in the materials.

Figures 2(e) and 2(f) show the optical properties of the dual-spun material across the solar spectrum and the mid-infrared wavelengths, respectively. In Figure 2(e), the spectral reflectance of PVDF-HFP and silica nanofibers are included for comparison, as well as those of double-aluminized Mylar and aluminum foil. Double-aluminized Mylar (D.A.M) is extensively used as a multilayer insulation (MLI) material for passive thermal management of spacecraft. D.A.M, which has similar radiative properties as aluminum foil, exhibits broadband behavior across a wide spectral range (particularly, a low infrared emissivity). This directly impacts the material's ability to self-cool in extraterrestrial conditions, a criterion important for the storage of cryogenic propellants. Conversely, the nanofibrous materials exhibit spectral selectivity, having very high reflectance in the 300 – 2500 nm

range of the solar spectrum, strong mid-infrared emittance, and would offer remarkable thermal management performance.

Comparing the three nanofibrous materials revealed slight differences in their optical properties. PVDF-HFP nanofibers recorded an average solar reflectance of 99.2% and an average infrared emittance of 86.5%. For silica nanofibers, the average solar reflectance and emittance were 96.6% and 89.5% respectively. The dual-spun PVDF-HFP-silica composite nanofibrous material exhibited slightly higher solar reflectance (96.9%) than silica, while it had an average emittance of 90.7%. Introducing silica nanofibers into the PVDF-HFP nanofibrous network led to a slight reduction in its solar reflectance due to the intrinsic optical characteristics of silica. A drop in solar reflectance (increase in solar absorptance) would imply an increase in the solar radiation absorbed, and consequently, an undesirable heat gain into the insulated system. However, this trade-off is offset by the preservation of the structural integrity of the network, to ensure long-term use of the material in the harsh environment of space, particularly in Low Earth Orbit. Despite the reduction in solar reflectance, there was an increase in the average emittance of the composite. This increase could directly relate to an increase in its self-cooling ability, which could compensate for any unwanted absorption of incident light and heat gain. Future studies would focus on studying the effects of different ratios of the constituent materials on the optical and structural properties of the resulting composite nanofibrous material.

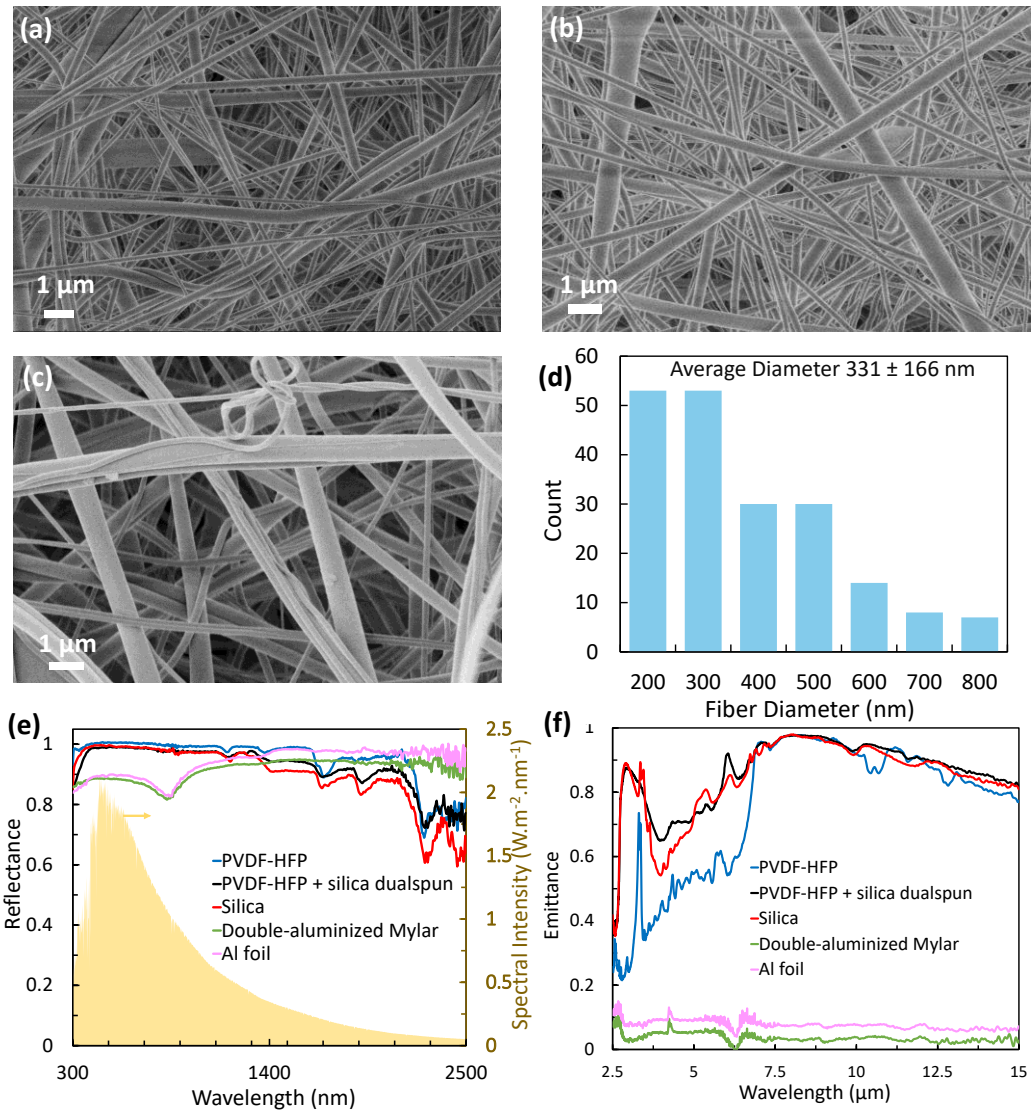

Figure 2. SEM image (at 25 K magnification) of (a) electrospun PVDF-HFP nanofibers, (b) electrospun silica nanofibers, and (c) dual electrospun PVDF-HFP -silica nanofibers. (d) Fiber diameter distribution of dual-spun PVDF-HFP – silica nanofibers. (e) Spectral solar reflectance of PVDF-HFP, silica, and dual-spun composite nanofibers. Double-aluminized Mylar and aluminum foil are included for comparison (f) Infrared spectral emittance of the samples at 300 K.

3.2 Atomic Oxygen and Thermal Cycling Effects

Despite the PVDF-HFP nanofibers' outstanding ability to reflect solar radiation, they experience some degradation in the presence of atomic oxygen (AO). Figure 3(a) depicts the materials' morphology and structure after 24 hours of exposure to plasma-generated atomic oxygen. Although the porous structure is preserved, which is important to allow multiple internal scatterings and strong diffuse reflectance, the thin nanoscale fibers coalesce into microfibers. This new structure would likely attenuate the exceptionally high solar reflectance of PVDF-HFP because the microfiber sizes are no longer comparable to the wavelengths at the peak of the solar spectrum, causing a reduction in the material's scattering and passive thermal control capabilities.

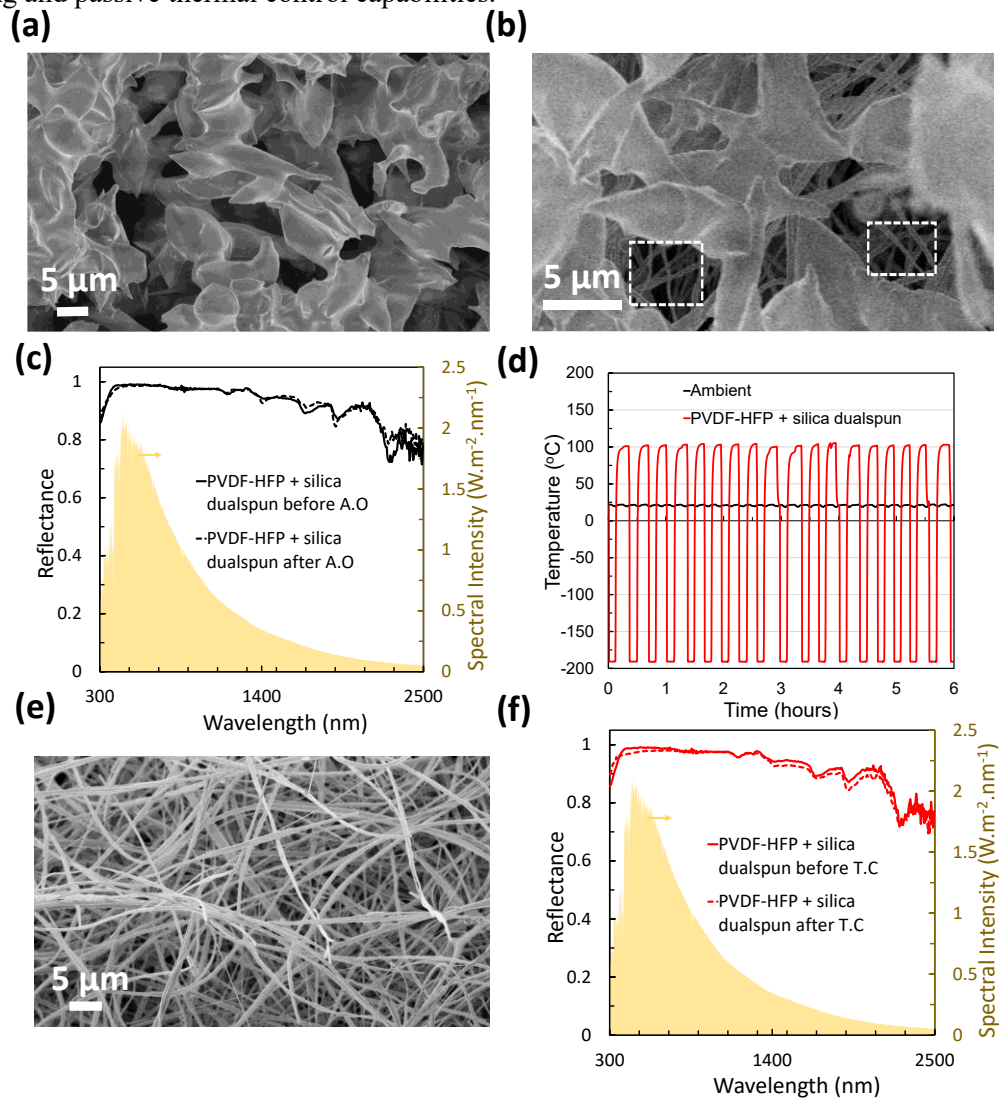

Figure 3. SEM image (at 5 K magnification) of (a) electrospun PVDF-HFP and (b) dual-spun PVDF-HFP – silica nanofibers after atomic oxygen exposure. (c) Spectral solar reflectance of the dual-spun PVDF-HFP – silica nanofibers after atomic oxygen exposure. (d) Temperature evolution with time during the thermal cycling

test. (e) SEM image (at 5 K magnification) of the dual-spun material after thermal cycling. (f) Spectral solar reflectance of the dual-spun PVDF-HFP – silica nanofibers after thermal cycling.

To address this concern, we augmented the PVDF-HFP nanofibers' atomic oxygen resistance by introducing silica nanofibers. Silica, a chemically stable and oxygen-saturated compound, would resist oxidation by atomic oxygen, being in its highest oxidation state. Introducing silica would help protect the internal structure of the polymeric PVDF-HFP nanofibers and ensure that the porosity of the nanofibrous composite is preserved after exposure to atomic oxygen. Additionally, the use of silica in nanofibrous form would also encourage diffuse scattering of incident light within the material, thereby preserving the strong solar reflectance. Figure 3(b) shows the dual-spun material after exposure to AO. The PVDF-HFP AO-conditioned microfibers are noticeable in the foreground of the image, while the smaller-sized silica nanofibers (annotated in Figure 3(b)) are visible in the background of the image. A clear distinction between the two images is that there are more pore spaces and fewer microscale fibers in Figure 3(b) after AO exposure, indicating that the silica nanofibers have likely played a significant role in maintaining the dual-spun material's internal structure. This observation is further strengthened by comparing the spectral solar reflectance of the dual-spun material before and after atomic oxygen exposure, as seen in Figure 3(c). By examining both spectra, we observe that there are minor variations in the spectral reflectance post-AO. The average solar reflectance of the dual-spun composite after AO was 96.8%, indicating a 0.1% decrease in the solar reflectance of the pristine sample. This slight reduction in the solar reflectance demonstrates the importance of enmeshing silica nanofibers in the PVDF-HFP nanofibrous network because it helps to prevent significant reductions in the reflectance by providing structural stability, preserving the porous network and allowing diffuse scattering of light off the nanofibers' surfaces. Further experiments will be conducted to provide insights into the effects of varying the concentration of the precursor materials on the atomic oxygen resistance of the composite material.

The thermal cycling experiment, conducted on the dual-spun material by alternating the thermal environment between cryogenic and hot conditions, Figure 3(d), reveals the material's stability and resistance to thermal swings. By closely observing Figure 3(e), we find that the material's porous structure is preserved after the temperature swings. The nanofibers do not appear to fracture under the thermal stresses, and they do not melt or coalesce into larger microfibers. Also, their smooth-textured morphology (noted in Figure 2(c)) remains unchanged after the thermal cycling experiment. Figure3(f) shows the spectral solar reflectance of the dual-spun composite before and after the thermal cycling experiment. The post-thermal cycling average solar reflectance was 96.2% (0.7% drop), underscoring the resistance of the dual-spun composite to thermal swings. Detailed characterization of the composite material's properties and testing are planned to study the material's ability to resist extreme environmental conditions.

4. Conclusions

In this study, we have used the dual electrospinning manufacturing method to combine PVDF-HFP polymeric nanofibers with ceramic-based silica nanofibers into a single network of nanofibers. This was done to improve the atomic oxygen resistance of the polymeric material, with the goal of not significantly affecting its superb solar reflectance and infrared emittance. The resulting composite nanofibrous material adopts a similar structure and morphology as its precursors, while retaining strong, albeit slightly decreased solar reflectance (compared to PVDF-HFP nanofibers). Preliminary experimental studies highlight the composite material's ability to resist thermal cycling-induced structural damage. The composite material also appears to retain its nanoporous structure post-exposure to atomic oxygen, exhibiting better resistance compared to PVDF-HFP nanofibers. These extreme conditions also do not induce significant changes in the composite material's average solar reflectance,

highlighting the material's ability to retain a strong radiative performance in extraterrestrial conditions. Continued investigation will involve more comprehensive experiments and material characterization to assess this current approach to manufacturing resilient thermal control nanofibers for extraterrestrial applications.

Acknowledgments
The authors acknowledge the support of the National Aeronautics and Space Administration under Grant No. 80NSSC21K0072 issued through the Space Technology Research Grants.

Declaration of Competing Interest
The authors declare the following financial interests/personal relationships, which may be considered as potential competing interests: Rensselaer Polytechnic Institute has filed the following non-provisional patent application related to this work – Non-Provisional Application No: 19/178,759.

References

[1] Ibekwe C, Wang X, Bolzani BN, O'Brien C, Waataja CJ, Mahony CP, et al. ACS Appl Mater Interfaces 2024. https://doi.org/10.1021/acsami.4c02463.
[2] Ibekwe, C, Wang, X, Hartwig, JW, Feller, JR, Swanger, AM, & Narayan, S. " *Proceedings of the ASME 2024 International Mechanical Engineering Congress and Exposition*. *Volume 9: Heat Transfer and Thermal Engineering*. Portland, Oregon, USA. November 17–21, 2024.ASME. https://doi.org/10.1115/IMECE2024-144206
[3] Ibekwe, C, Wang, X, Hartwig, JW, Swanger, AM, & Narayan, S." *Proceedings of the ASME 2024 International Mechanical Engineering Congress and Exposition*. *Volume 9: Heat Transfer and Thermal Engineering*. Portland, Oregon, USA. November 17–21, 2024. ASME. https://doi.org/10.1115/IMECE2024-146008
[4] Banks BA. MISSE-Flight Facility Polymers and Composites Experiment 1-4 (PCE 1-4). 2021.
[5] Banks, B. A. (ed.). (2014). *Spacecraft Polymers Atomic-Oxygen Durability Handbook* (NASA-HDBK-6024, Change 2, published 27 Jun 2014). NASA Technical Handbook.
[6] De Groh KK, Banks BA. MISSE 2 Peace Polymers Erosion Morphology Studies. n.d.
[7] Banks BA. Atomic Oxygen Erosion Data From the MISSE 2-8 Missions. 2019.
[8] De Groh KK, Banks BA, Santo L. Materials International Space Station Experiment-9 (MISSE-9) Polymers and Composites Experiment. n.d.
[9] Parisi G, Szewczyk PK, Narayan S. Wettability gradient of photoresponsive electrospun yarns for harp-based fog water harvesting 2024. https://doi.org/10.1016/j.xcrp.2024.102176.
[10] Parisi G, Szewczyk PK, Narayan S, Stachewicz U. Photoresponsive Electrospun Fiber Meshes with Switchable Wettability for Effective Fog Water Harvesting in Variable Humidity Conditions. ACS Appl Mater Interfaces 2023;15. https://doi.org/10.1021/acsami.3c07044.
[11] Parisi G, Szewczyk PK, Narayan S, Ura DP, Knapczyk-Korczak J, Stachewicz U. Multifunctional Piezoelectric Yarns and Meshes for Efficient Fog Water Collection, Energy Harvesting, and Sensing. Small Science 2024;4. https://doi.org/10.1002/smsc.202400021.
[12] Miller SKR, Banks BA, Waters DL. Investigation into the differences between atomic oxygen erosion yields of materials in ground-based facilities and LEO. High Perform Polym, vol. 20, 2008, p. 523–34. https://doi.org/10.1177/0954008308089711.
[13] Banks BA, Dill GC, Loftus RJ, De Groh KK, Miller SK. Comparison of Hyperthermal Ground Laboratory Atomic Oxygen Erosion Yields With Those in Low Earth Orbit. NASA/ TM—2013-216613.
[14] Stambler, A. H., Inoshita, K. E., Roberts, L. M., Barbagallo, C. E., De Groh, K. K., & Banks, B. A. (2011). *Ground-Laboratory to In-Space Atomic Oxygen Correlation for the Polymer Erosion and Contamination Experiment (PEACE) Polymers.* NASA/TM—2011-216904.
[15] Dorodnyy A, Smajic J, Leuthold J. Mie Scattering for Photonic Devices. Laser Photon Rev 2023;17. .